



## Evaluation of Antimicrobial Activity Using Cadmium Oxide Nanoparticles Prepared by Physical Method (PLAL)

Tuqa A. Khaleefa<sup>1\*</sup>  and Nisreen kh. Abdalameer<sup>2</sup> 

<sup>1,2</sup>Department of Physics, College of Science for Women, University of Baghdad, Baghdad, Iraq.

\*Corresponding Author

Received: 14 September 2023

Accepted: 19 November 2023

Published: 20 January 2025

[doi.org/10.30526/38.1.3716](https://doi.org/10.30526/38.1.3716)

### Abstract

The present study employed the pulsed laser ablation in liquid (PLAL) technique to synthesize cadmium nanoparticles (CdO NPs). PLAL is a top-down physical method that operates by splitting the precursor mass of metal ions into metal atoms. This work utilized a nanosecond Nd-YAG laser with two wavelengths, specifically 1064 nm and 532 nm, at a laser energy of 250 mJ. 250 pulses were applied for each wavelength during the synthesis process. This approach enabled the production of high-purity nanoparticles. The characteristics of the nanoparticles that were created were examined by the use of UV-Vis, and XRD analysis techniques. The antibacterial and antifungal properties of the tested substance were evaluated against two Gram-positive bacteria, namely Staphylococcus aureus and Streptococcus mutans, as well as two Gram-negative bacteria, specifically Escherichia coli and Pseudomonas aeruginosa. These bacterial strains were obtained from the oral cavity. Additionally, a specific genus of fungi known as Candida exists. The findings of the study indicate that CdO NPs synthesized using the PLAL technique possess antibacterial properties, rendering them effective in eradicating pathogenic bacteria and fungi

**Keywords:** Antibacterial, Antifungal, cadmium oxide, Nd-YAG, pulsed laser ablation in liquid.

### 1. Introduction

The utilization of laser ablation in deionized water has been extensively employed for the synthesis of metallic, bi-metallic, and tri-metallic nanoparticles, in addition to metal oxides (1). One notable benefit associated with the utilization of laser technology for nanoparticle synthesis is the attainment of nanoparticles with a much-elevated level of purity, distinct surface charge properties, and simplified preparation procedures when compared to conventional chemical approaches (2). The manipulation of nanoparticle size distribution and shape can be achieved by the use of several laser parameters, including laser power (3).

energy density (fluence), beam spot size, scanning speed, medium in which ablation occurs, and wavelength. Various studies have employed nanosecond and picosecond lasers of distinct



wavelengths to generate diverse categories of nanoparticles (4), albeit the utilization of picosecond lasers remains limited in the existing literature (5). The experimental results demonstrated that the creation of nanoparticles at a wavelength of 1064 nm resulted in the formation of smaller spherical particles and a greater production rate compared to the production at a wavelength of 533 nm. Moreover, the experimental results demonstrated that an increase in laser energy led to enhanced productivity and the generation of bigger nanoparticles (6).

The researcher studied the effect of using a nanosecond laser with varying laser wavelengths and laser effectiveness on the synthesis of palladium (Pd) nanoparticles in distilled water (7). Additionally, it was demonstrated that the plasma temperature associated with the longer wavelength exhibited a significantly greater magnitude compared to that of the shorter wavelength. This disparity can be attributed to the heightened inverse Bremsstrahlung reaction rate, which effectively contributes to the thermalization of the induced plasma (8). Furthermore, the observation of the blue shift phenomenon at the extended laser wavelength provides evidence indicating that the plasma generated at 1064 nm possesses higher energy levels compared to the plasma generated at 193 nm (9). The present study investigated the impact of employing a nanosecond laser with varying laser wavelengths and laser fluence on the synthesis of palladium (Pd) nanoparticles in distilled water (10).

The study revealed that Pd nanoparticles generated using wavelengths of 532 nm and 355 nm exhibit greater homogeneity and lower dimensions compared to those produced using a wavelength of 1064 nm (11). The findings of the study indicate that there is a direct relationship between the rise in laser fluence and the corresponding increase in nanoparticle size across all wavelengths (12).

Cadmium oxide is classified as an inorganic compound with the chemical formula Cd-O (13). The oxidation of elemental cadmium in the presence of air results in the formation of CdO, a compound consisting of cadmium and oxygen (14). CdO is classified as an n-type semiconductor and is a member of the II-VI binary system (15). The material has crystal formations that manifest as either brown or crimson hues or as an amorphous colorless powder.

Cadmium oxide (CdO) exhibits promising characteristics as a prospective candidate owing to its low band gap of 2.5 eV, refractive index of 2.49, and notably high conductivity in the range of 4 to 5 (16). The material finds extensive use in a diverse array of applications, encompassing photovoltaics, phototransistors, gas catalysis, and chemical sensing, among others (17). CdO NPs have gained significant recognition in the field of optoelectronics, particularly in the applications of phototransistors, photodiodes, and photovoltaic devices (18). Cadmium oxide nanoparticles (CdO NPs) have also demonstrated novel applications in the fields of cancer cell eradication and medication delivery (19). Cadmium oxide nanoparticles (CdO NPs) have noteworthy antibacterial efficacy against a wide range of pathogenic microorganisms that have developed resistance to conventional antibiotics. The user has provided a numerical range of (20). In this study, a pulsed laser ablation technique in liquid with varying laser parameters was used to manipulate the laser settings to achieve nanosynthesis of cadmium oxide and subsequently investigate its physical properties, as well as its antibacterial and antifungal efficacy.

## 2. Materials and Methods

Cadmium oxide nanoparticles (CdO NPS) were synthesized through the pulsed laser ablation technique in liquid (PLAL). A pure cadmium plate with dimensions of (1 x 1) mm was immersed in 6 ml of deionized water with a purity of 99.99% in a beaker. The plate was positioned at a

distance of 7 cm from the laser source, where a Q-switched Nd-YAG laser was utilized. The laser operated at a repetition rate of 8 Hz and emitted wavelengths of (1064, and 532) nm, with an energy of 250 mJ. The experimental setup is illustrated in **Figure 1**. A total of 250 pulses were applied for each wavelength. Subsequently, the samples underwent both structural and optical analyses.

The solution's antibacterial and antifungal properties were subsequently evaluated against two strains of Gram-positive bacteria (*Staphylococcus aureus*, *Streptococcus mutans*), two strains of Gram-negative bacteria (*Escherichia coli*, *Pseudomonas aeruginosa*), and *Candida* fungi. This was accomplished by employing the drilling technique, wherein a volume of 10 mL of the solution was introduced into the cavity. The agar diffusion method was employed to evaluate the impact of CdO nanoparticles on the bacterial strains utilized. This experimental procedure involves the application of bacterial samples onto agar plates, followed by a designated incubation period. Subsequently, sterile micropipette tips were employed to create perforations in the agar medium, followed by the introduction of a mixing solution into the created apertures (21).

Following the incubation period, the inhibitory potency was assessed by measuring the diameters of the inhibition zones from numerous directions using a ruler, and this process was repeated multiple times. The aforementioned bacteria were utilized after their acquisition, which involved the processes of isolation, classification, and cultivation. These procedures can be succinctly described as follows: the bacteria were collected from infected individuals, subjected to standard techniques for separation and classification to determine their respective types, and subsequently cultivated on nutrient-rich culture media(22). Throughout these steps, strict adherence to sterile methods and maintenance conditions was ensured. Finally, the bacteria were preserved through freezing until they were ready for use. The particles that had been generated were afterward assessed for their capacity to impede the growth of these bacteria. This was achieved by introducing them into an agar medium within Petri dishes, utilizing the drilling technique to create holes in the agar, and subsequently depositing the solution containing the particles into these holes. The Petri dishes were then placed in a basin and incubated for a period of 24 hours. **Table 1** shown laser parameters and characteristics.

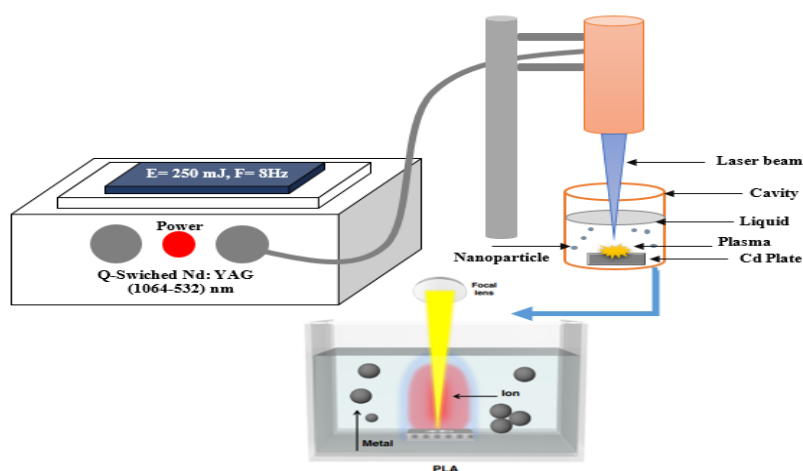


**Figure 1.** A schematic diagram illustrating the process of pulsed laser ablation in liquid (PLAL) for the synthesis of nanoparticles (NPs).

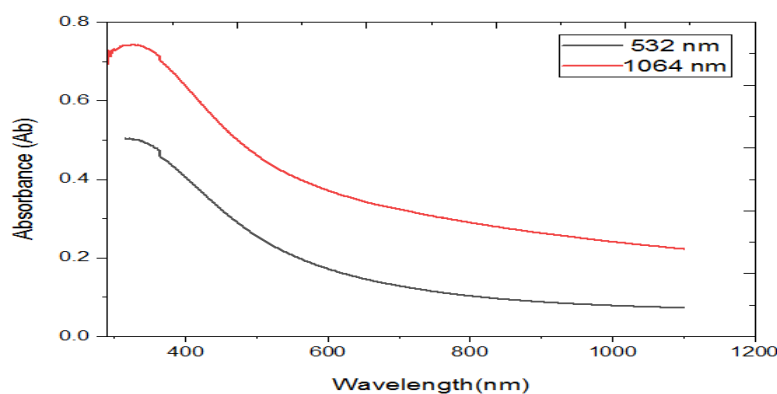
**Table 1.** Laser parameters of the nanosecond laser at both wavelengths (532 and 1064 nm).

Laser parameters	$\lambda = (1064, 532) \text{ nm}$
Pulse energy	250 mJ
Number of pulsed	250 P
Frequency	8 Hz
Pulse duration	10 ns

### 3. Results and Discussion

#### 3.1 Optical Analysis

The technique described is extensively employed to identify a diverse range of substances, including transition metal ions, chemical compounds, and biological components. The initial indication of a synthesis reaction is observed through the alteration in color of cadmium colloidal solutions. Initially colorless, the solutions gradually transition to a light grey hue, which further intensifies with an increasing number of pulses due to the cadmium ablation process. The initial characterization of CdNPs and their oxides was conducted using UV-Vis analysis. The highest absorption at (300, 317) nm was recorded in **Figure 2** while utilizing the (1064, 532) nm Nd-YAG laser, with a corresponding number of pulses of 250, **Table 2** shown in the optical analysis of CdO NPs.

**Figure 2.** Absorbance function wavelength at (1064, and 532) nm.**Table 2.** Optical analysis for FHG, and SHG laser.

E= 250 mJ, F= 8 Hz, No. pulses= 250 P	
Harmonic generation (nm)	Max wavelength (nm)
1064	300
532	317

The two laser wavelengths employed, namely 532 nm and 1064 nm, exhibit distinct energy levels that are attributed to them. Shorter wavelengths, such as 532 nm, exhibit greater photon energy in comparison to longer wavelengths, such as 1064 nm. At a wavelength of 532 nm, the laser emits photons possessing comparatively greater energy. Semiconductor nanoparticles demonstrate energy levels that are dependent on their size, which includes the energy level of the bandgap. The bandgap energy refers to the minimum amount of energy needed to facilitate the transition of an electron from the valence band to the conduction band. When CdO nanoparticles are synthesized using a laser with a wavelength of 532 nm, a portion of the photons with high energy is absorbed by the CdO nanoparticles. The process of absorbing high-energy photons can

facilitate the transition of electrons from the valence band to the conduction band, resulting in the formation of excitons, which are electron-hole pairs.

Excitons, upon formation, lead to a reduction in the population of electrons within the valence band, hence inducing a pronounced decline in the absorption spectrum. The utilization of a 532 nm laser induces the excitation of electrons confined within the CdO nanoparticles, hence diminishing their capacity to absorb photons within the visible spectrum. Consequently, this leads to a discernible decrease in the optical absorption spectrum.

At a wavelength of 1064 nm, the laser emits photons with a lesser energy in comparison to the wavelength of 532 nm. The lower-energy photons may lack sufficient energy to directly induce the transition of electrons from the valence band to the conduction band within the CdO nanoparticles. On the contrary, it is plausible that the 1064 nm laser predominantly induces thermal effects, leading to the elevation of temperature in both the CdO nanoparticles and their immediate surroundings. The heightened thermal energy has the potential to induce structural alterations or generate vibrations in both the CdO nanoparticles and the encompassing media. The observed first rise in the absorption spectrum could perhaps be attributed to alterations in the structural characteristics of the nanoparticles or the interplay between the nanoparticles and their immediate surroundings. As time progresses, the absorption spectrum gradually diminishes as the system attains a new state of equilibrium.

Cadmium oxide nanoparticles (NPs) were synthesized in the samples prepared within the scope of this study. To determine the energy gap ( $E_g$ ) of these oxides, we analyzed them by plotting the absorption as a function of wavelength, as depicted in **Figure 3** to calculate the energy gap, we employed the Tauc Equation (23 ,24).

$$\alpha h\nu = \beta(h\nu - E_g)^m \tag{1}$$

The constant  $\beta$  exhibits variability in value, which is contingent upon the specific transitions being considered. The symbol  $E_g$  represents the energy gap,  $h\nu$  represents the photon energy, and  $m$  is a constant with a value of  $1/2$  that corresponds to direct permitted transmission in semiconductors.

By graphing  $(\alpha h\nu)^2$  as a function of photon energy  $h\nu$  and extrapolating the linear portion of the curve to intersect the  $h\nu$  axis at the point  $(\alpha h\nu)^2 = 0$ , the resulting intersection point shows the energy gap. The provided figure, labeled as **Figure 3**, illustrates the correlation between the square of the product of the fine structure constant ( $\alpha$ ) and the photon energy ( $h\nu$ ) for films composed of cadmium oxide. **Table 3** shown in the energy gap of CdO NPs.

**Table 3.** Energy gap for FHG, and SHG laser.

<b>E= 250 mJ, F= 8 Hz, No. pulses= 250 P</b>	
<b>Harmonic generation (nm)</b>	<b>Energy gap (eV)</b>
1064	2.5
532	2.75

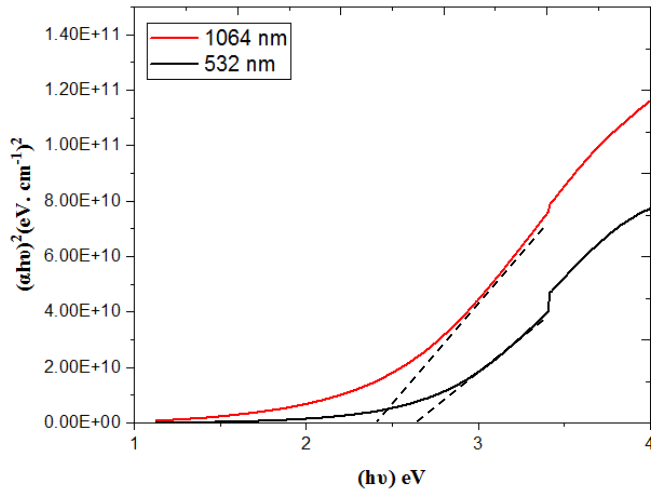


**Figure 3.** Energy gap for CdO NPs at (1064, and 532) nm.

The laser ablation wavelength employed during the creation of cadmium nanoparticles (CdO NPs) has the potential to exert an influence on their energy gap. In the present scenario, the user has indicated that CdO nanoparticles (NPs) synthesized through laser ablation at a wavelength of 532 nm exhibit an energy gap of 2.75 eV, whereas those synthesized through laser ablation at a wavelength of 1064 nm exhibit an energy gap of 2.5 eV. The observed disparity can be ascribed to a multitude of variables(13). The dimensions and arrangement: The size and structure of nanoparticles can vary based on the conditions of ablation.

The bandgap of nanoparticles is inversely related to their size, with smaller nanoparticles exhibiting broader bandgaps and larger nanoparticles displaying narrower bandgaps. The selection of laser wavelength has the potential to influence the size distribution of the CdO NPs. The energy levels exhibited by CdO nanoparticles (NPs) are subject to modulation as a result of variations in their size and surface states. Variations in laser wavelength can induce alterations in the energy levels of nanoparticles, thereby influencing the energy gap.

The surface states of nanoparticles exhibit variability contingent upon the process employed for their synthesis. The presence of surface states has the potential to capture or release charge carriers, hence exerting an influence on the total energy bandgap of the material. The phenomenon of quantum confinement becomes increasingly significant in nanoparticles as their size diminishes. The utilization of various laser wavelengths can lead to distinct levels of quantum confinement, hence influencing the energy gap. The laser wavelength can exert an influence on the crystal structure of CdO NPs. Various crystal forms exhibit distinct electrical properties, which encompass variations in energy gap.

### 3.2 Structure Analysis

**Figure 4** displays the X-ray diffraction pattern obtained from the production of CdO nanoparticles. The cubic phase of CdO, as indicated by the JCPDS (ARD NO 01-104), has distinct peaks at 30°, 37°, 44°, 46°, and 56°, which correspond to the (311), (331), (422), (511), and (531) planes, respectively. The presence of distinct peaks in the X-ray diffraction (XRD) spectrum indicates a high degree of crystallinity in the CdO nanoparticle. The calculation of the crystalline size  $D$  of the synthesized CdO nanoparticle is performed using Scherrer's formula (25)(26).

$$D = \frac{0.9 \lambda}{\beta \cos \theta} \quad (2)$$

In this context,  $D$  represents the crystalline size,  $\lambda$  denotes the wavelength of the X-ray employed,  $\Delta 2\theta$  refers to the width of the diffraction line measured at half of its greatest intensity, and  $\theta$  represents the angle of diffraction. The crystallin protein family. This graphic illustrates the crystal systems, angles, and Miller's visibly evident index. The phenomenon of laser-induced oxidation is an inevitable outcome resulting from the interaction between lasers and metals in the presence of atmospheric oxygen. This phenomenon arises due to the elevated temperatures encountered by the metal that is directly subjected to the laser. The dissipation of heat to the surrounding environment rapidly transforms into a process whereby heat spreads to the nearby region, resulting in the oxidation of a metal area that extends beyond the directly exposed and ablated channel. The findings indicate that the chemical composition of metal surfaces undergoes alterations based on the net transmitted fluency. The observed pattern exhibits a notable surge in oxygen concentration at lower levels of laser fluency, succeeded by a gradual approach towards a maximum value at higher fluencies.

Peaks were identified at wavelengths of  $30^\circ$ ,  $37^\circ$ , and  $56^\circ$ , which could perhaps be attributed to the presence of the glass substrate. In this case, it is shown that both spectra exhibit identical characteristics, suggesting that variations in wavelengths do not impact the crystalline structures of the CdO nanoparticles.

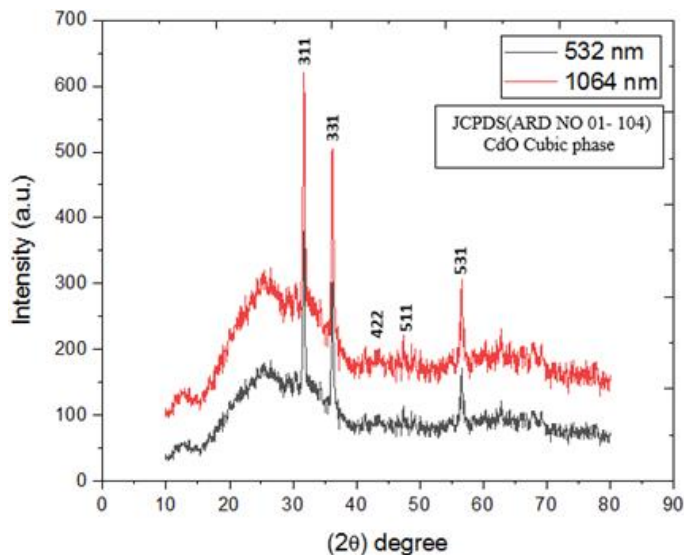


**Figure 4.** XRD pattern for CdO NPs at (1064, 532) nm.

**Table 4.** Crystalline size for CdO NPs at FHG, and SHG laser.

E= 250 mJ, F= 8 Hz, No. pulses= 250 P		
Harmonic generation (nm)	Crystalline size (nm)	hkl
1064	22.90	311
	24.99	331
	24.21	531
532	23.29	311
	25.75	331
	24.88	531

### 3.3 Anti-Microbial Activity

The generation of antibacterial drugs with exceptionally high activity was achieved using the

physical synthesis of CdO nanoparticles. **Figure 5** presents the analysis of several dosages administered for the treatment of human multidrug-resistant infections. The illnesses considered in this study include Gram-positive bacteria such as *Staphylococcus aureus* and *Staphylococcus epidermidis*, as well as Gram-negative bacteria like *Escherichia coli* and *Klebsiella*. Additionally, the examination also encompasses the impact of these dosages on the fungal pathogen *Candida*. The experiment was conducted within a controlled clinical environment, where the pathogens were successfully separated. The diameter of the inhibitory zone, which was a focal point of this study, is presented in **Table 5**.

The results of the experiment indicated that bacteria associated with *Staphylococcus aureus* exhibited a greater presence in inhibitory zones compared to bacteria associated with *Escherichia coli*. One possible explanation for this difference is the distinct composition of the cell walls of these two organisms. Nanoparticles of cadmium oxide (CdO) were synthesized using physical means utilizing polylactic acid (PLA) as a precursor. These CdO nanoparticles demonstrated significant antibacterial efficacy across different types, exhibiting comparable levels of activity. The size range of these nanoparticles typically fell between 0.2 and 100 nm. The enhanced antibacterial efficacy of nanoparticles can be attributed to their increased interaction with bacteria due to their small size (27).

Nanoparticles exhibit efficacy by perturbing the electron transport chain and impeding the transmission of energy across bacterial membranes. This is how they operate. Several investigations have demonstrated that the antimicrobial activity of nanoparticles against Gram-negative bacteria is attributed to their ability to penetrate and disrupt the integrity of the bacterial cell walls (28). The attack leads to an alteration in the permeability of the cell membrane. Consequently, the regulation of chemical transport across the cytoplasmic membrane of bacterial cells is a significant challenge, leading to the eventual demise of the cell. The generation of free radicals and the consequent impairment of the cytoplasmic membrane, stemming from the formation of these free radicals, have been postulated as the underlying mechanisms behind the antibacterial efficacy of nanoparticles. The demonstrated antibacterial capabilities of nanoparticles provide support for this hypothesis. At a wavelength of 1064 nm, the highest proportion of positive bacterial inhibition was observed (29).

**Table 5.** Inhibition zone for CdO NPs at FHG, and SHG laser.

E= 250 mJ, F= 8 Hz, No. pulses= 250 P		
Harmonic generation (nm)	Microorganisms	Inhibition zone (mm)
1064	<i>Staphylococcus aureus</i>	21
	<i>Staphylococcus epidermidis</i>	14
	<i>Escherichia coli</i>	0
	<i>Klebsiella</i>	0
	<i>Candida</i>	15
532	<i>Staphylococcus aureus</i>	14
	<i>Staphylococcus epidermidis</i>	13
	<i>Escherichia coli</i>	0
	<i>Klebsiella</i>	0
	<i>Candida</i>	14

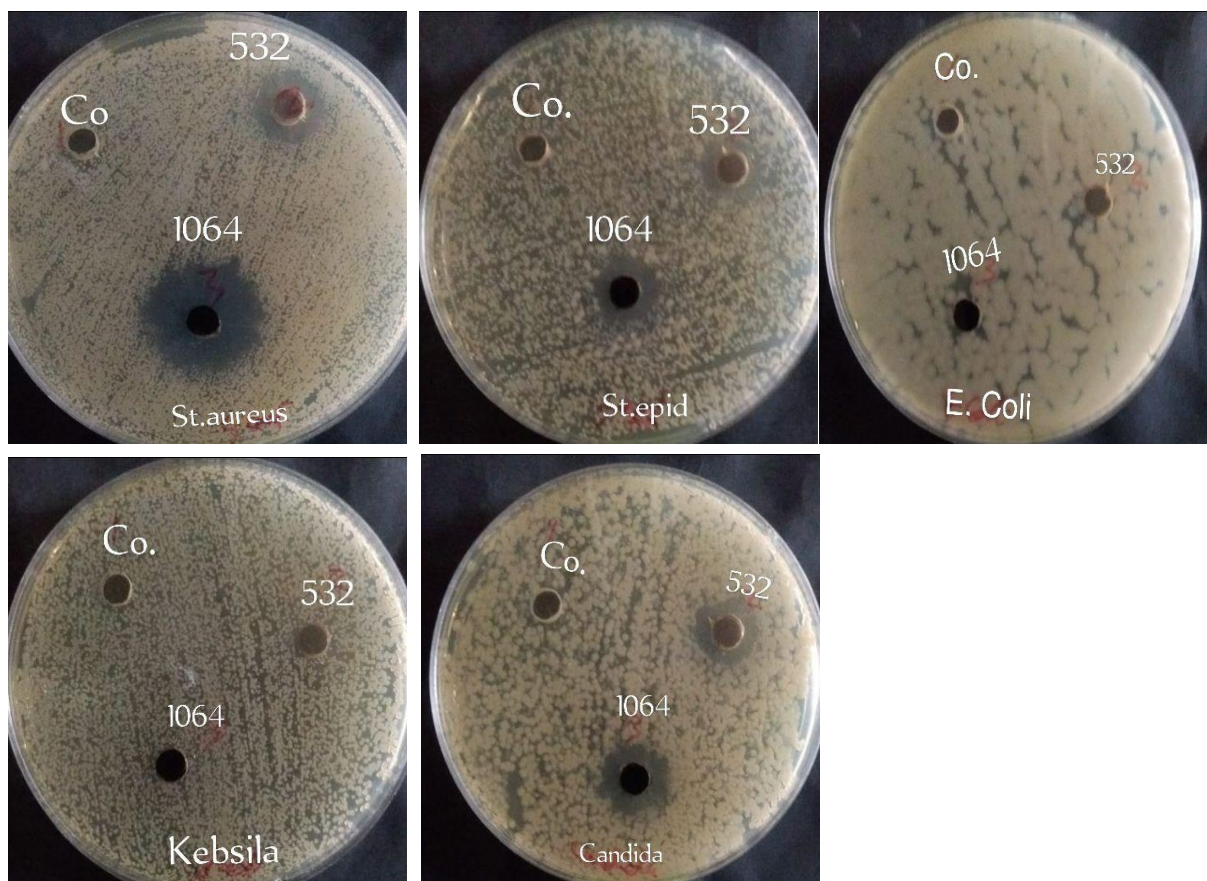


**Figure 5.** Antimicrobial activity for CdO NPs at (1064, 532) nm.

#### 4. Conclusion

This study explored the feasibility of synthesizing CdO nanoparticles through pulsed laser ablation in liquid (PLAL). CdO nanoparticles demonstrated antibacterial activity, and synthesis was achieved using two Nd: YAG laser wavelengths (1064 nm and 532 nm). The study found that samples synthesized at 1064 nm were most effective. These CdO nanoparticles exhibited antibacterial properties and in vitro cytotoxic effects, warranting further investigation into their toxicity mechanisms. PLAL was deemed a convenient method for metal nanoparticle synthesis, offering a promising alternative to existing techniques with demonstrated biological effectiveness. However, further research is needed to explore the impact of modifying laser parameters and examining additional variables for practical applications.

#### Acknowledgment

We thank the Medical Physics Lab., Department of Physics, College of Science for Women, University of Baghdad.

#### Conflict of Interest

No conflict of interest.

#### Funding

We hereby confirm that all the Figures and Tables in the manuscript are ours. Furthermore,

any Figures and images, that are not ours, have been included with the necessary permission for re-publication, which is attached to the manuscript.

### Ethical Clearance

The project was approved by the local ethical committee at the University of Baghdad.

### References

1. Baig N, Kammakam I, Falath W, Kammakam I. Nanomaterials: A review of synthesis methods, properties, recent progress, and challenges. *Mater Adv*. 2021;2(6):1821–71. <https://doi.org/10.1039/d0ma00807a>.
2. Abdalameer NK, Mazhir SN. Cytotoxic activity of Green Zinc Selenide Nanoparticles Against Hep-G2 Cell Lines. *Indian J Forensic Med Toxicol* [Internet]. 2021 Jan 7;15(1):207–218. <http://dx.doi.org/10.37506/ijfmt.v15i1.13713>.
3. Geoffrion L, Hesabizadeh T, Medina-Cruz D, Kuser M, Taylor P, Vernet-Crua A, et al. Naked Selenium Nanoparticles for Antibacterial and Anticancer Treatments. *ACS Omega*. 2020 Feb 5;5(6):2660–9. <https://doi.org/10.1021/acsomega.9b03172>
4. Khalaph KA, Abdalameer NK, Mousa AQ. Study the physical properties of CdSe nanostructures prepared by a pulsed laser deposition method Study the Physical Properties of CdSe Nanostructures Prepared by a Pulsed Laser Deposition Method. 2021;130023(November). <https://doi.org/10.1063/5.0065731>
5. You A, Be M, In I. Generation of nanoparticle colloids by picosecond and femtosecond laser ablations in liquid flow. *Appl Phys Lett*. 2021;083113(October):1–4. <http://dx.doi.org/10.1063/1.2773937>
6. Yao H, Asamoah E, Wei P, Cong J, Zhang L, Quaisie JK, et al. Investigation into the effect of increasing target temperature and the size of cavity confinements on laser-induced plasmas. *Metals* (Basel). 2020;10(3). <https://doi.org/10.3390/met10030393>
7. Chen X, Li P, Dun Y, Song T, Ma B. Nanosecond-pulsed Q-switched Nd : YAG laser at 1064 nm with a gold nanotriangle saturable absorber. *Appl Phys B lasers Opt* [Internet]. 2018;124(92):1–5. Available from: <http://dx.doi.org/10.1007/s00340-018-6952-7>.
8. Fikry M, Tawfik W, Omar MM. Investigation on the effects of laser parameters on the plasma profile of copper using picosecond laser induced plasma spectroscopy. *Opt Quantum Electron* [Internet]. 2020;52(5):1–16. Available from: <https://doi.org/10.1007/s11082-020-02381-x>
9. Liu HC, Mao XL, Yoo JH, Russo RE. Early phase laser induced plasma diagnostics and mass removal during single-pulse laser ablation of silicon. *Spectrochim acta, Part B At Spectrosc*. 1999;54(11): 607–24. [https://doi.org/10.1016/S0584-8547\(99\)00092-0](https://doi.org/10.1016/S0584-8547(99)00092-0)
10. Fan G, Qu S, Wang Q, Zhao C, Zhang L. Pd nanoparticles formation by femtosecond laser irradiation and the nonlinear optical properties at 532 nm using nanosecond laser pulses Pd nanoparticles formation by femtosecond laser irradiation and the nonlinear optical properties at 532 nm using nanos. *J Appl Phys*. 2011;109(023102):1–9. <https://doi.org/10.1063/1.3533738>
11. Kim KK, Kim D, Kim SK, Park SM, Song JK. Formation of ZnO nanoparticles by laser ablation in neat water. *Chem Phys Lett* [Internet]. 2011;511(1–3):116–20. Available from: <http://dx.doi.org/10.1016/j.cplett.2011.06.017>
12. Wang J, Li X, Wang C, Zhang L, Li X. Effect of laser wavelength and energy on the detecting of trace elements in steel alloy. *Optik (Stuttg)*. 2018 Aug 1;166:199–206. <http://dx.doi.org/10.1016/j.ijleo.2018.04.018>
13. Murbat HH, Abdalameer NKH, Brrd AK, Abdulameer F. Effects of Non-Thermal Argon Plasma Produced at Atmospheric Pressure on the Optical Properties of CdO Thin Films. *Baghdad Sci J* [Internet]. 2018 Jun 4;15(2):0221. <http://dx.doi.org/10.21123/bsj.2018.15.2.0221>
14. Ubale AU, Wadnerkar SS, Tayade PNSGD. Study of structural, optical and electrical properties of

- CdO thin film deposited by sol-gel spin coating technique. 2014;5(6):43–8. <https://link.springer.com/article/10.1007/s10971-017-4412-1>
15. Shehab AAA, Salih AA. The Optical Properties of Aluminum Doped CdO Thin Films Prepared by Vacuum Thermal Evaporation Technique. *Ibn Al-Haitham Jour Pure Appl Sci.* 2014;27(3):279–90.
  16. Ajar SHS, Ahmad EYA, Hussein EAA, Habib AAH. Study the Effect of Irradiation on Structural and Optical Properties of ( CdO ) Thin Films that Prepared by Spray Pyrolysis. *Ibn Al-Haitham J Pure Appl Sci.* 2015;28(2):41–51.
  17. Habubi NF, Abraham BA, Noore ES. Influence of Irradiation on some Optical Properties of ( CdO ) Thin Films Prepared by Spray Pyrolysis. 2017;74(30):15–21. <http://dx.doi.org/10.56431/p-oqp90x>
  18. Abdulameer NK. Impact of Dielectric Barrier Discharge ( DBD ) Plasma on the Optical Properties of Thin Films. 2020;15(8):1937–42.
  19. Hussein EH, Mohammed NJ, Al-Fouadi AHA, Abbas KN, Alikhan JS, Maksimova K, et al. Impact of deposition temperature on the structural properties of CdS/Si nanoparticles for nanoelectronics. *Mater Lett.* 2019;254. <https://doi.org/10.1016/j.matlet.2019.07.088>
  20. Naser GY, Raja WN, Faris AS, Rahem ZJ, Salih A, Ahmed AH. Some optical properties of CdO thin films. *Energy Procedia [Internet].* 2013;36:42–9. <http://dx.doi.org/10.1016/j.egypro.2013.07.006>
  21. Razuqi NS, Muftin FS, Murbat HH, Abdalameer NK. Influence of dielectric-barrier discharge (DBD) cold plasma on water contaminated bacteria. *Annu Res Rev Biol.* 2017;14(4). <https://doi.org/10.9734/ARRB/2017/34642>
  22. Abdalameer NK, Khalaph KA, Ali EM. Ag/AgO nanoparticles: Green synthesis and investigation of their bacterial inhibition effects. *Mater Today Proc [Internet].* 2021;45(xxxx):5788–92. Available from: <https://doi.org/10.1016/j.matpr.2021.03.166>.
  23. Abdalameer NK, Mazhir SN, Aadim KA. The effect of ZnSe Core/shell on the properties of the window layer of the solar cell and its applications in solar energy. *Energy Reports [Internet].* 2020;6(April):447–58. Available from: <https://doi.org/10.1016/j.egy.2020.09.023>.
  24. Hassanien AS, Aly KA, Akl AA. Study of optical properties of thermally evaporated ZnSe thin films annealed at different pulsed laser powers. *J Alloys Compd.* 2016;685(November 2018):733–42. <http://dx.doi.org/10.1016/j.jallcom.2016.06.180>
  25. Abbas EM, Mazhir SN, Abdalameer N kh. In Vitro Evaluating Antimicrobial Activity for MgO Nanoparticles Prepared by PLAL. *Int J Nanosci.* 2022;21(6):1–6. <http://dx.doi.org/10.1142/S0219581X2250048X>
  26. Hasaneen MF, Alrowaili ZA, Mohamed WS. Structure and optical properties of polycrystalline ZnSe thin films: Validity of Swanepol’s approach for calculating the optical parameters. *Mater Res Express.* 2020;7(1). <https://doi:10.1088/2053-1591/ab6779>
  27. Niema AAR, Abbas EM, Abdalameer NK. Enhanced antibacterial activity of selenium nanoparticles prepared by cold plasma in liquid. *Dig J Nanomater Biostructures.* 2021;16(4):1479–85. <http://dx.doi.org/10.15251/DJNB.2021.164.1479>
  28. Sabah N. Mazhir, Nisreen Kh. Abdalameer JKH. Cold plasma synthesis of Zinc Selenide Nanoparticles for inhibition bacteria using disc diffusion. *Phys Chem Solid State.* 2022;23(4):652–8. <http://dx.doi.org/10.15330/pcss.23.4.652-658>
  29. Shanan ZJ, Abdalameer NK, Ali HMJ. Zinc Oxide Nanoparticle Properties and Antimicrobial Activity. *Int J Nanosci [Internet].* 2022 Jun 20;21(03):1–6. Available from: <https://doi/10.1142/S0219581X2250017X>.
  30. Murali KR, Kalaivanan A, Perumal S, Pillai N. Sol-gel dip coated CdO:Al films. *J. Alloys Compd.* 2010;503(2):350-353.